JACS
JOURNAL OF THE AMERICAN CHEMICAL SOCIETY

Article

pubs.acs.org/JACS

Operative Mechanism of Hole-Assisted Negative Charge Motion in Ground States of Radical-Anion Molecular Wires

Carlos Franco,[†] Paula Mayorga Burrezo,[‡] Vega Lloveras,[†] Rubén Caballero,[§] Isaac Alcón,[∥] Stefan T. Bromley,[*,∥,⊥] Marta Mas-Torrent,[†] Fernando Langa,[§] Juan T. López Navarrete,[‡] Concepciò Rovira,[*,†] Juan Casado,[*,‡] and Jaume Veciana[*,†]

[†]Department of Molecular Nanoscience and Organic Materials, Institut de Ciència de Materials de Barcelona (ICMAB-CSIC)/CIBER-BBN, Campus Universitari de Bellaterra, Cerdanyola, E-08193 Barcelona, Spain

[‡]Department of Physical Chemistry, University of Malaga, Campus de Teatinos s/n, 29071 Malaga, Spain

[§]Instituto de Nanociencia, Nanotecnología y Materiales Moleculares (INAMOL), University of Castilla-La Mancha, Campus de la Fábrica de Armas, 45071 Toledo, Spain

[∥]Department of Materials Science and Physical Chemistry, Faculty of Chemistry, University of Barcelona, Avenida Diagonal, 647, 08028 Barcelona, Spain

[⊥]Catalan Institution of Research and Advanced Studies (ICREA), 08010 Barcelona, Spain

Supporting Information

ABSTRACT: Charge transfer/transport in molecular wires over varying distances is a subject of great interest. The feasible transport mechanisms have been generally accounted for on the basis of tunneling or superexchange charge transfer operating over small distances which progressively gives way to hopping transport over larger distances. The underlying molecular sequential steps that likely take place during hopping and the operative mechanism occurring at intermediate distances have received much less attention given the difficulty in assessing detailed molecular-level information. We describe here the operating mechanisms for unimolecular electron transfer/transport in the ground state of radical-anion mixed-valence derivatives occurring between their terminal perchlorotriphenylmethyl/ide groups through thiophene−vinylene oligomers that act as conjugated wires of increasing length up to 53 Å. The unique finding here is that the net transport of the electron in the larger molecular wires is initiated by an electron−hole dissociation intermediated by hole delocalization (conformationally assisted and thermally dependent) forming transient mobile polaronic states in the bridge that terminate by an electron−hole recombination at the other wire extreme. On the contrary, for the shorter radical-anions our results suggest that a flickering resonance mechanism which is intermediate between hopping and superexchange is the operative one. We support these mechanistic interpretations by applying the pertinent biased kinetic models of the charge/spin exchange rates determined by electron paramagnetic resonance and by molecular structural level information obtained from UV−vis and Raman spectroscopies and by quantum chemical modeling.

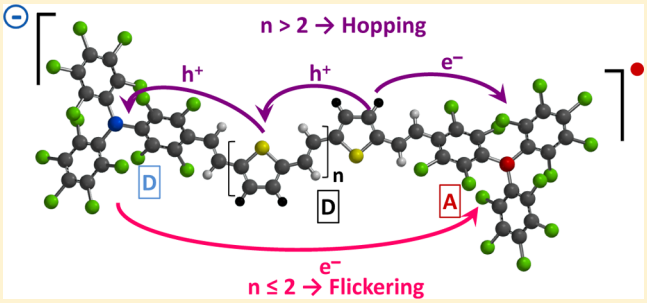

INTRODUCTION

The main mechanisms used to describe charge transfer/transport processes across a chain of ionizable molecular subunits are charge hopping (CH), flickering resonance (FR), and superexchange (SE).[1] CH is a thermally activated incoherent process where a localized charge excess is assumed to hop between consecutive sites on the bridge where relaxation takes place previous to each hop. In this model "real" wire states (i.e., excited, conformational, charged, hot vibrational, etc.) take an active part in the charge transport, and for this reason, this mechanism is operative even for long bridges. On the contrary, the SE mechanism occurs owing to the energy alignment of the levels of the two terminal subunits (resonance) which causes the charge to tunnel from one extreme of the wire to another without residence on the bridge. Thereby this mechanism is operative only for the shorter wires. Finally, the recently proposed FR[1] mechanism can be thought of as a compromise between CH and SE where the energy levels of the two terminal subunits and those of the bridge subunits become all in resonance due to thermal fluctuations. Then, the charge moves ballistically, without nuclear relaxation, through the energy-aligned states to become trapped at the end of the wire. Given the inherent nature of charge transfer/transport, it combines and competes with many other molecular processes, thus giving rise to a panoply of scenarios. In order to understand such complex phenomena, which are particularly relevant in molecular electronics and biological

Received: August 18, 2016
Published: December 20, 2016

DOI: 10.1021/jacs.6b08649
J. Am. Chem. Soc. 2017, 139, 686−692

systems, detailed knowledge from a range of experimental and theoretical probes is of vital importance.

The most commonly employed protocol for mechanistic studies of charge transport is the measurement of electrical currents through molecular junctions.[2−9] However, complementary *in situ* spectroscopic studies are difficult given the nanometer resolution often required. For analogous studies in solution, molecular charge transport in donor−bridge−acceptor compounds is usually evaluated by photoexcitation on the donor forming a adiabatic charge transfer state which relaxes in an energetically downhill movement of the charge through the wire, whereby its dynamics can be studied by time-resolved spectroscopies.[10] Unfortunately, these photoactivated transient methods also contain coupling terms among the excited states, thus potentially "masking" the intrinsic charge transport characteristics in the ground state.[11,12] It turns out that "clean" insights into the intrinsic conduction mechanisms are obtained in the unperturbed ground electronic state for which mixed-valence (MV) systems are very good choices. Among these, radical MV systems are ideal candidates for this purpose since they can be studied by means of electron paramagnetic resonance (EPR) in solution[13] which, in addition, facilitates the use of complementary *in situ* spectroscopic techniques, like UV−vis−NIR and Raman, providing further rich molecular level cross-information.

Perchlorotriphenylmethyl radicals (PTM) are persistent and stable open-shell derivatives with good electron accepting properties and have been successfully used as redox centers in MV radical-anion systems, allowing the study of electron transfer/transport through different bridges.[14−16] Bridges based on thiophene-vinylene oligomers (***n*TV**) have been recently demonstrated to perform as one of the most efficient π−conjugated extended molecular wires.[17−19] Given their electron-rich donor nature, these ***n*TV** bridges are typically considered as hole (positive charge) transmitters.[17−19] Conversely, ***n*TV** bridges have never been used to promote charge transfer/transport between negatively charged terminal groups.

In this work, a series of six electron-donor ***n*TV** oligomers,[17] substituted at their terminal sites with two PTM radical groups, **$^{\bullet}$PTM-*n*TV-PTM$^{\bullet}$** (Scheme 1), properly reduced to radical-anion MV species are studied. The excess charge conduction behavior in the resulting mixed-valence **[PTM-*n*TV-PTM]$^{\bullet-}$** species is studied by variable-temperature EPR complemented by *in situ* UV−vis−NIR and resonant Raman spectroscopies and supported by electronic structure calculations. This multifold information on the spin/charge exchange rate in the ground electronic states serves for the longer oligomers (***n*TV**; n = 4−7) to propose a biased bidirectional symmetrical charge-hopping mechanism through the ***n*TV** bridge, imparted by two reflecting PTM sites at opposite ends. The initial step of the mechanism is the thermally activated intramolecular oxidation of the donor wire by the acceptor "neutral" **PTM$^{\bullet}$** subunit forming a symmetric charge-separated state with a mobile positive polaron in the bridge flanked by two **PTM^{-}** anions. After the formation of this transitory positive polaronic species, the charge may hop among the TV units and finally decays by an electron−hole annihilation that restores the neutrality of the ***n*TV** bridge in the radical anion. This finding is rather unusual since charge transport of negative charge (**PTM$^{\bullet-}$ → PTM$^{\bullet}$**) through hole transmitter bridges (***n*TV**) mostly occurs through empty "conduction" states able to accommodate an excess of charge rather than mediated by positive charges. On the contrary, in the shorter radical-anions (***n*TV**; n = 2, 3) the operative mechanism for the spin/charge exchange seems to be the FR mechanism favored by the higher rigidity (or quinoidization) of their bridges.

Scheme 1

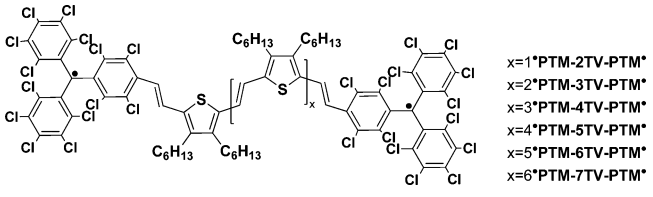

RESULTS AND DISCUSSION

Synthesis and Characterizations. The synthesis of diradicals **$^{\bullet}$PTM-*n*TV-PTM$^{\bullet}$** (n = 2−7) starts with the preparation of the corresponding hydrogenated derivatives, **(αH,α′H)-PTM-*n*TV-PTM**, through a Wittig Horner olefination between the polychlorotriphenylmethane phosponate derivative[20] and the suitable ***n*TV** dialdehydes (see Supporting Information). Treatment with an excess of base gives the corresponding biscarbanions **[PTM-*n*TV-PTM]$^{-2}$** that are subsequently oxidized to **$^{\bullet}$PTM-*n*TV-PTM$^{\bullet}$**. Diradicals **$^{\bullet}$PTM-*n*TV-PTM$^{\bullet}$** were completely characterized with usual spectroscopic techniques, like IR, UV−vis (Table S1), Raman, and MALDI-TOF MS (see Supporting Information). Cyclic voltammetries of diradicals **$^{\bullet}$PTM-*n*TV-PTM$^{\bullet}$** show well-resolved two-electron reduction peaks and reversible oxidations resulting in amphoteric redox behaviors of **$^{\bullet}$PTM-*n*TV-PTM$^{\bullet}$** (Table S2). Solution EPR spectra of diradicals **$^{\bullet}$PTM-*n*TV-PTM$^{\bullet}$** (Table S3) consist of four overlapped main lines from which two isotropic hyperfine coupling constants, a_i, that are half of those observed for the segmental model monoradical **PTM-2TV** (see Supporting Information). Such results indicate the existence of a magnetic interaction between the two unpaired electrons through the diamagnetic bridge, which are additionally confirmed by frozen solution EPR spectra of **$^{\bullet}$PTM-2TV-PTM$^{\bullet}$** and **$^{\bullet}$PTM-3TV-PTM$^{\bullet}$** (Figure 1a) that show ΔM_s = 2 half-field forbidden transitions due to thermally accessible triplet states (Figures S65−S70). Generation of radical-anions **[PTM-*n*TV-PTM]$^{\bullet-}$** was achieved by a stepwise chemical or electrochemical reduction of diradicals **$^{\bullet}$PTM-*n*TV-PTM$^{\bullet}$**.

***In Situ* Spectroscopic Studies.** Intramolecular spin/charge transfer in radical-anions **[PTM-*n*TV-PTM]$^{\bullet-}$** was examined by variable-temperature EPR measurements. In all these radical-anions, the EPR profiles changed with the temperature going from four to three overlapped lines when the temperature is increased (in the range 200−300 K), indicating a passage from the slow to fast exchange regime at the EPR time-scale. The first-order rate constants (k) for spin/charge exchange between the two PTM sites in each compound were determined by simulation of the experimental EPR spectra using the ESR-EXN software[21] (Figures 1a and S2−S7). The comparison at a given temperature for all radical anions demonstrates that k decreases with the increasing of the ***n*TV** bridge length (Figure 1b). For a given compound, k also exhibits a net dependence with the temperature (Figure 1b) disclosing that a thermally activated intramolecular dynamic spin/charge exchange occurs between the two terminal PTM sites for all radical-anions. From the

DOI: 10.1021/jacs.6b08649
J. Am. Chem. Soc. 2017, 139, 686−692

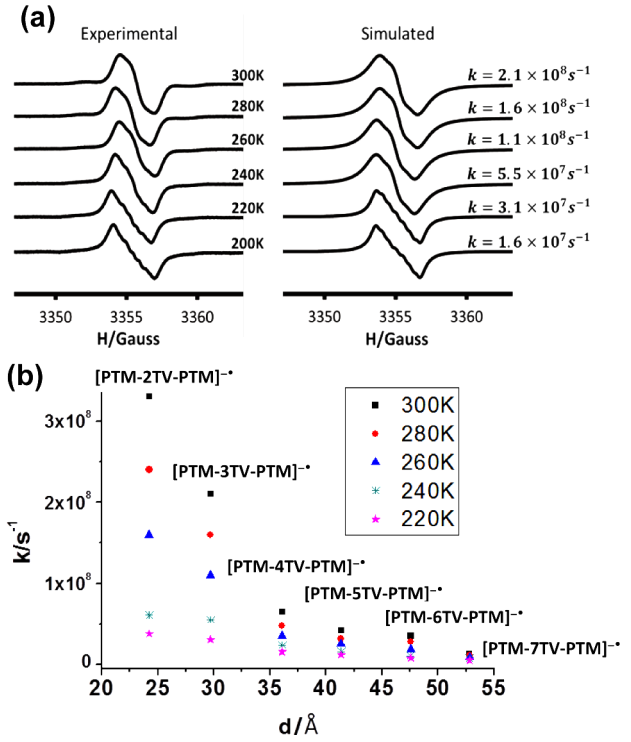

Figure 1. (a) Temperature-dependent changes in the EPR spectrum of [**PTM-3TV-PTM**]$^{\bullet-}$**NBu**$_4^+$ solution in CH_2Cl_2 (left), obtained by chemical reduction with $NBu_4^+OH^-$, and simulated spectra (right) with different spin/charge exchange rates. (b) Distance dependences of spin/charge exchange rates, *k*, of radical-anions [**PTM-*n*TV-PTM**]$^{\bullet-}$ in the temperature range 220−300 K.

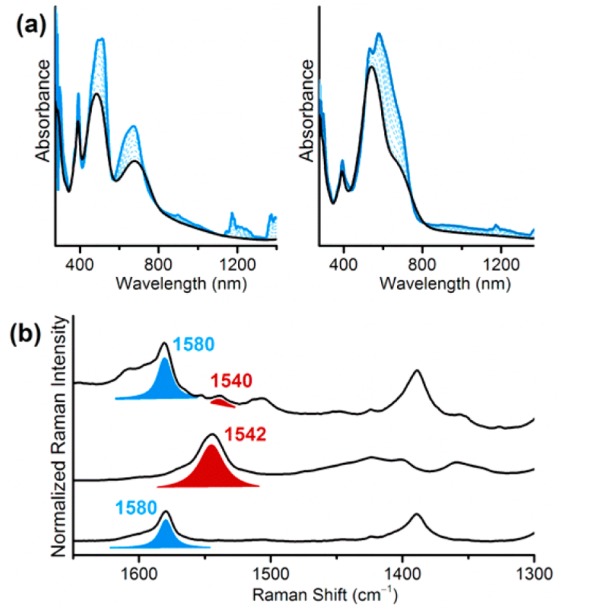

Figure 2. (a) Evolution of UV−vis−NIR spectra of the [**PTM-2TV-PTM**]$^{\bullet-}$**NBu**$_4^+$ (left) and [**PTM-5TV-PTM**]$^{\bullet-}$**NBu**$_4^+$ (right) as a function of the temperature, obtained by chemical reduction with $NBu_4^+OH^-$. Solid black line corresponds to UV−vis−NIR at room temperature and solid blue line at 77K. (b) Comparison of 633 nm Raman spectra in DCM of [**PTM-4TV-PTM**]$^{\bullet-}$**NBu**$_4^+$ (top), [**PTM-4TV-PTM**]$^{\bullet+}$**Cl**$^-$ (medium) and $^{\bullet}$**PTM-4TV-PTM**$^{\bullet}$ (bottom).

thermal dependence of *k* values we deduced that for the shorter compounds the operating mechanism is strongly dependent on the temperature as well as on the length of the bridge, whereas for the longer ones both thermal and size variations are considerably smaller. Such different behaviors between shorter (***n*TV**; n= 2, 3) and longer (***n*TV**; *n* = 4−7) bridges point to the presence of two different mechanisms. The question about the particular electron transfer/transport mechanism which operates in these MV radical-anions is therefore pertinent.

Variable-temperature UV−vis−NIR electron absorption spectroscopy under the same conditions as the EPR measurements, were performed for all radical-anions. Spectra at room temperature (Figures 2a and S8) show three well-distinguished kinds of bands: a band at around 390 nm, characteristic of a **PTM**$^{\bullet}$ radical chromophore, another set of very intense bands at 485−573 nm (***n*TV** centered bands), due to the conjugated ***n*TV** bridges, and finally absorption bands with medium intensity at 678−720 nm, assigned to the negatively charged **PTM**$^-$ partially spreading out in the bridge (i.e., forming the PTM&***n*TV** segment). Worth noticing is the intervalence charge transfer (IVT) band exhibited by [**PTM-2TV-PTM**]$^{\bullet-}$ at 1372 nm (Figure S1 inset) which is not detected for the rest of radical-anions. This result is consistent with the typical exponential decay of the intensity (accompanied by a blue-shift) of IVT bands with increasing molecular lengths that makes the IVT band to be hidden by the PTM anion and ***n*TV** bands.

Interestingly, the ***n*TV** centered bands of radical-anions clearly show a red-shift with the enlargement of the bridge from 485 to 573 nm, while the PTM&***n*TV** absorption is less altered with the size (i.e., from 678 nm for [**PTM-2TV-PTM**]$^{\bullet-}$ to 720 nm in [**PTM-7TV-PTM**]$^{\bullet-}$). Furthermore, the ***n*TV** bands are broad and ill-resolved at room temperature but evolving into a clear vibronic structure at 77K which are more pronounced in the larger compounds (Figure 2a and S8). Conversely, the rest of the bands (from PTM chromophores and PTM&***n*TV** segments) are minimally affected by cooling. The detection of vibrational resolution in the absorption spectra on cooling might reveal the existence of an ample distribution of molecular conformers at room temperature formed by distortions among the repeating units around the thiophene vinylene C−C bonds. By removing the thermal energy the population of the most planar, rigid, and energetically stable conformer is increased providing the vibronic components. Furthermore, this indicates the flatness or flexibility of the ground electronic state potential energy curve against conformational distortions in the larger MV radical-anions, an aspect of relevance for the further discussion.

Resonant Raman spectra of radical-anions [**PTM-*n*TV-PTM**]$^{\bullet-}$ at room temperature (Figures 2b, top, and S9) taken with the excitation laser at 633 nm, in resonance with one of the absorption bands of the radical anion, provide their unique vibrational fingerprints. In comparison with the Raman spectra of the neutral diradicals (Figures 2b, bottom, and S10), radical-anions (Figures 2b, top, and S9) exhibit resonant Raman bands emerging from their different domains: (i) The bands at >1600 cm^{-1} are due to PTM-***n*TV** fragments mostly supporting the excess of negative charge. (ii) The bands at 1580−1590 cm^{-1} corresponding to the molecular fraction of the bridge without an excess of negative charge, as previously reported.[22] Nevertheless, the most significant finding in these resonant Raman spectra is the detection of bands with medium-low intensities around 1540 cm^{-1}, together with several other weaker bands in the region of 1390−1460 cm^{-1}. In Figure 2b, the spectrum of the radical cation [**PTM-4TV-PTM**]$^{\bullet+}$

DOI: 10.1021/jacs.6b08649
J. Am. Chem. Soc. 2017, 139, 686−692

(generated from $^{\bullet}$**PTM-4TV-PTM**$^{\bullet}$ by addition of one equivalent of a $FeCl_3$ solution) is also shown which presents the most prominent band at 1540 cm^{-1} accompanied be weaker features in the same interval of 1390−1460 cm^{-1}, such as that in [**PTM-4TV-PTM**]$^{\bullet-}$. In the [**PTM-4TV-PTM**]$^{\bullet+}$, the charge is confined in the middle of the ***n*TV** moiety (the electro-deficient **PTM**$^{\bullet}$ at each extreme repels the positive charge), and the thiophenes get quinoidal. However, the vinylenes are correspondingly strained, overall planarizing the bridge. Indeed, the resemblance between the 1540/1390−1460 cm^{-1} bands in [**PTM-4TV-PTM**]$^{\bullet+}$ and [**PTM-4TV-PTM**]$^{\bullet-}$ reveals common structural features.

Mechanistic Analysis. To elucidate the mechanism of electron transfer, one often refers to the interpretation of the k values within the framework of the classical Marcus theory which includes the role of the temperature in connection with microscopic parameters of relevance such as reorganization energies, electronic couplings and driving forces. We propose that the mechanism of the spin/charge exchange, at least in the larger radical-anions [**PTM-*n*TV-PTM**]$^{\bullet-}$(n = 4−7), proceeds as shown in Scheme 2 (see also Scheme S5) where a hole is

Scheme 2

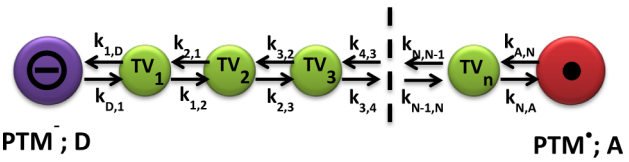

stepwise transported by a hopping mechanism along the ***n*TV** molecular wire. The election of this sequential mechanism is first justified since it takes into account the electron acceptor capability of PTM radical unit and the donor ability of ***n*TV** bridges as revealed by their amphoteric redox behavior. This redox property supports the simultaneous presence of the negative and positive charges (charge separated state) in the molecule. Assuming a hole in the ***n*TV** bridge, this simplified kinetic scheme can be described as a biased symmetrical bidirectional hopping of the positive charge process with two reflecting sites at the opposite molecular ends where the rates of site-to-site hopping inside the ***n*TV** toward ($k_1 = k_{2,1}$) and away ($k_2 = k_{1,2}$) from the terminal PTM units are different but identical to those rates of the other wire extreme ($k_1 = k_{2,1} = k_{N-1,N}$ and $k_2 = k_{1,2} = k_{N,N-1}$) as required by the molecular symmetry (see Supporting Information for more details). In particular, we assume that $k_1 > k_2$[23] because the rate of a hole moving toward a nearby negatively charged PTM site must be larger than that in the opposite direction due to electrostatic attraction. In addition, we assume that the hopping rates backward and forward inside the wire are similar ($k_{N-1,N-2} = k_{N-2,N-1} = k_3$; $\forall\ N \geq 4$) because the hopping hole is far from the charged termini. According to the classical Marcus theory and previous considerations on related systems,[24,25] the apparent spin/charge exchange rate k_{ET} is given by (see Supporting Information):

$$k_{ET} \simeq \frac{\pi}{\hbar}\frac{|V_{D1}|^2}{\sqrt{4\pi\lambda_D k_B T}}\, e^{-(\Delta E_{BD}+\lambda_{D1})^2/4\lambda_{D1}k_B T}\, e^{-\beta(R-R_0-2r)} \quad (1)$$

where ΔE_{BD} is the energy change corresponding to an electron injection from the TV bridge site nearest to PTM$^{\bullet}$ radical to the latter site (transition TV1→ PTM$^{\bullet}$), λ_{D1} (= λ_{AN}) is the reorganization energy of such a transition, $|V_{D1}|$ (= $|V_{AN}|$) denotes the coupling of the PTM$^{\bullet}$ to the corresponding terminal unit of the bridge, k_B the Boltzman's constant, T the absolute temperature, R (in Å) is the overall distance over which the spin/charge is transferred, R_0 corresponds to the distance between the PTM units separated by a single-bridging TV unit (17.9 Å), r is the distance between two neighboring TV units (4.6 $Å^{-1}$), and β ($Å^{-1}$) is the decay factor. R and R_0 values for all radical anions were determined as the distances between the central carbon atoms of the PTM units, obtained by quantum chemical calculations from the optimized geometries. The solution of eq 1 is linked to the underlying mechanism by means of ΔE_{BD} which is therefore inserted in the equation as a phenomenological parameter characteristic of the proposed mechanism. In our case, ΔE_{BD} represents the energy cost for the formation of a transient intermediate species which should contain a positive polaron in the middle of the ***n*TV** structure and therefore flanked by two PTMs each one with a negative charge. Assuming this, the barrier is accounted by the free energy required to form the dianion−cation charge separated state which is provided by the Weller formalism.[26] This formalism considers the cathodic and anodic redox potentials for the independent formation of a radical cation and a radical-anion and are directly taken from the CV data (see Supporting Information) in accordance with the donor character of the ***n*TV** bridges (Table S2)[17,27] and the acceptor nature of PTM radical units.[28] This approximation gave ΔE_{BD} values from +1.13 eV for the shorter (n = 2) to +0.83 eV for the larger (n = 7) radical anion (see Supporting Information). Finally, fitting the experimental k data of [**PTM-*n*TV-PTM**]$^{\bullet-}$ (n = 4−7) to eq 1 using the latter ΔE_{BD} values gave the following parameters: $\lambda_{D1} = \lambda_{AN} \approx 0.5$ eV, $|V_{D1}| = |V_{AN}| \approx 0.07$ eV, and a decay factor β of 0.25 $Å^{-1}$. These values are fully consistent with our experimental observations: (i) Since $\lambda_{1A} > |V_{1A}|$, therefore all radical-anion systems can be classified as class II MV systems. (ii) The moderate decay factor value is in consonance with the capacity of the wire of transmitting the charge through large distances between the redox centers by means of a hopping mechanism. It must be highlighted that this mechanism conciliates the amphoteric redox behavior, and the detection in the Raman spectrum of the anion radical species of a weak feature which is due to the radical cation at the bridge (or dianion−cation species) and the rigidity at low temperatures of the bridge because of the contributions of the thienoquinoidal polarons.

Theoretical Modeling. To provide more insight into the underlying charge transfer phenomena, density functional theory (DFT) calculations were performed on [**PTM-2TV-PTM**]$^{\bullet-}$ where the spectator C_6H_{13} side chains of the TV units were replaced by methyl groups to reduce computational cost. For improved agreement with experiment, previous studies of molecular MV systems have recommended using functionals 50% of Hartree−Fock-like exchange (HFLE)[29] or 35% HFLE together with a continuum treatment of solvation and a 6-311G ++ basis set.[30] We found that both approaches yielded stable charge localized states and here, unless otherwise stated, we report results obtained using the PBE functional[31] with 50% HFLE (referred to as PBE-50) employing the Gaussian 09 code.[32] Unfortunately, similar calculations on larger radical-anions were untractable due to the large sizes of molecules. The optimized structure of [**PTM-*n*TV-PTM**]$^{\bullet-}$ (Figure 3a)

DOI: 10.1021/jacs.6b08649
J. Am. Chem. Soc. 2017, 139, 686−692

displays the 2TV bridge with a planar conformation and each PTM twisted by 40° with respect to the 2TV plane.

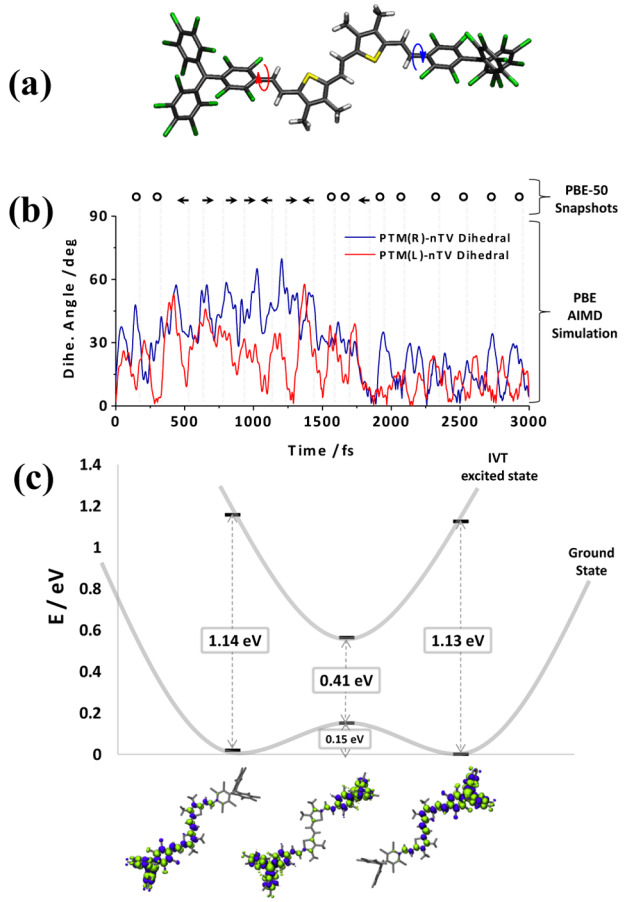

Figure 3. (a) Optimized structure of [**PTM-2TV-PTM**]$^{\bullet-}$. The helical arrows indicate the dihedral angles (φ) between each PTM unit and the 2TV wire. (b) Variation of the indicated dihedral angles in (a) during 3 ps of an AIMD simulation of [**PTM-2TV-PTM**]$^{\bullet-}$ at 300 K using the PBE functional. The left/right arrows and circles indicate left/right localization or delocalization of spin density respectively for particular tested snapshots with the PBE-50 functional. (c) Relative energies for each studied electronic configuration (left − localized, middle − delocalized, right − localized) in the corresponding relaxed conformations as obtained by PBE-50 optimizations. The calculated energies of the optical IVT (represented by the β-HOMO/β-SUMO gap) for each case are also provided. The structures of each configuration with the corresponding highlighted spin densities are provided below the x axis of panel c.

To assess the electron transfer/transport of [**PTM-2TV-PTM**]$^{\bullet-}$ at finite temperatures, we performed an *ab initio* molecular dynamics simulation (AIMD) at 300 K during 4 ps (1 ps of equilibration plus 3 ps of production) using the PBE functional, the Bussi−Donadio−Parrinello thermostat[33] and a light numerical basis set as implemented in the FHI-AIMS code.[34] From 18 sample "snapshots" of thermally activated conformations taken over a 3 ps period from these runs, we calculated the spin distribution using the PBE-50 method described above. As indicated in Figure 3b (top), during the thermal motion at 300 K the spin distribution fluctuates between being either localized on one of the two PTM units (← or →) or fully delocalized over the entire molecule (○). Figure 3b also plots the variation of the dihedral twist angle (φ) between each PTM unit and the 2TV wire. During the first 1.5 ps, φ presents large values, typical of highly twisted structures, and the spin distribution in [**PTM-2TV-PTM**]$^{\bullet-}$ tends to be localized on either one PTM unit (← or →). Conversely, for the latter 1.5 ps, φ values are much smaller (i.e., flatter conformation), and the spin distribution tends to delocalize over the entire molecular skeleton. Therefore, it seems that the spin density (and thus the negatively charged density) follows the thermally activated rotational fluctuations of [**PTM-2TV-PTM**]$^{\bullet-}$, in accordance with previous studies on single PTMs.[35] To investigate the 0 K potential energy landscape underlying the thermally perturbed conformers, we fully optimized the structures of the 18 snapshots using the PBE-50 method resulting in localized solutions in all cases. This suggests that the thermally excited structures with delocalized electronic states correspond to transitional conformations. The 0 K delocalized solution obtained from a highly symmetric structure is found 0.15 eV above all obtained localized solutions, providing a thermally accessible energy barrier between the localized electronic configurations (Figure 3c). Moreover, we have found that the β-HOMO/β-SUMO gap which we take as a reasonable approximation to the optical IVT energy depends on the degree of localization/delocalization of the ground electronic state. Specifically, we find that this gap ranges from 1.1 eV for the localized solutions to 0.4 eV for the transitional delocalized states, reproducing quite well the observed band appearing at 0.7 eV (i.e., 1372 nm). We further note that the experimental IVT value is also consistent with typical β-HOMO/β-SUMO gap values found for the 18 thermally activated snapshots.

According to the DFT results, the charge transfer mechanism for the shortest radical anion [**PTM-2TV-PTM**]$^{\bullet-}$ appears not to involve a net bridge polaron state but a transition state dependent on a resonance between the two PTM units, a situation more reconcilable with a SE mechanism. In pure SE, however, the bridge only plays a virtual role in the charge transfer, but in the case here our analysis reveals that the degree of coupling between the PTM units and the bridge (via the dihedral angles, φ) plays an essential role. Thus, a pure SE interpretation does not fully capture our theoretical findings. Between SE and hopping, the FR model aims to reconcile bridge participation without the presence of localized polarons on the bridge. We feel that for [**PTM-2TV-PTM**]$^{\bullet-}$ the FR mechanism is a reasonable alternative while for longer molecules the bridge will increasingly have more conformational freedom potentially allowing for charge/structure localization (i.e., polaron formation). In turn, this allows polaronic hopping to become increasingly prominent with respect to FR for bridges of $n \geq 3$ in [**PTM-*n*TV-PTM**]$^{\bullet-}$.

CONCLUSIONS

The use of a multitechnique approach, based on variable-temperature EPR, UV−vis−NIR, resonant Raman spectroscopies, and theoretical calculations, allowed us to thoroughly investigate the charge transfer mechanisms in the ground state of a series of six radical-anions [**PTM-*n*TV-PTM**]$^{\bullet-}$ (n = 2−7) of distinct lengths. For the shortest 2TV-bridged molecule we propose that charge transfer occurs through a flickering resonance type mechanism. On the contrary for molecules with bridges with 4 or more TV units, we propose that the exchange of the negative spin/charge occurs through a thermally activated incoherent biased bidirectional symmetrical charge hopping mechanism of positive charge. In this latter

DOI: 10.1021/jacs.6b08649
J. Am. Chem. Soc. 2017, 139, 686−692

mechanism, the transient polaron formation inside the bridge and the hopping of holes among the bridging TV units participate in the spin/charge exchange between the two terminal PTM units. The reported results show that a bridge with an electron-rich donor nature typically considered as an efficient hole transmitter can also be used to promote charge transfer/transport between neutral negatively charged terminal groups of molecular wires in their ground states.

■ ASSOCIATED CONTENT

Supporting Information

The Supporting Information is available free of charge on the ACS Publications website at DOI: 10.1021/jacs.6b08649.

Synthesis of dialdehyde ***n*TV** bridges; general procedure for the synthesis of **(αH,α′H)-PTM-*n*TV-PTM**, the segmental model **(αH)-PTM-2TV**, radical **2TV-PTM•**, and diradicals **•PTM-*n*TV-PTM•** (n = 2−7); EPR and CV data of radical **2TV-PTM•** and diradicals **•PTM-*n*TV-PTM•** (n = 2−7); CV of representative **(αH,α′H)-PTM-*n*TV-PTM**; vis−NIR of cations of diradical **•PTM-4TV-PTM•** and the model bridge; procedure for the generation of radical-anions $[\mathbf{PTM\text{-}}n\mathbf{TV\text{-}PTM}]^{\bullet-}$ (n = 2−7) and VT-EPR, UV−vis−NIR, and Raman spectra; kinetic model and rate data of spin/charge exchange process of radical-anions $[\mathbf{PTM\text{-}}n\mathbf{TV\text{-}PTM}]^{\bullet-}$($n$ = 2−7); ^{1}H NMR, ^{13}C NMR, FT-IR, MALDI-MS and EPR spectra of all new compounds (PDF)

■ AUTHOR INFORMATION

Corresponding Authors

*E-mail: s.bromley@ub.edu.
*E-mail: cun@icmab.es.
*E-mail: casado@uma.es.
*E-mail: vecianaj@icmab.es.

ORCID

Fernando Langa: 0000-0002-7694-7722
Jaume Veciana: 0000-0003-1023-9923

Notes

The authors declare no competing financial interest.

■ ACKNOWLEDGMENTS

We acknowledge the financial support from the Spanish MINECO/FEDER (grants CTQ2013-40480-R, CTQ2016-7989-R, and CTQ2015-64618-R), Spanish Ministry of Economy and Competitiveness, through the "Severo Ochoa" Programme for Centres of Excellence in R&D (grant SEV-2015-0496), the Generalitat de Catalunya (grants 2014SGR-17, 2014SGR-97, and XRQTC). We also acknowledge supercomputing resources provided by the Red Española de Supercomputacion and the Networking Research Center of Bioengineering, Biomaterials and Nanomedicine (CIBER-BBN). The work carried out at the University of Malaga was supported by MINECO/FEDER through the reference projects CTQ2012-33733 andCTQ2015-69391-P. The "Servicios Centrales de Apoyo a la Investigación" of the University of Malaga are also acknowledged by generous access to its facilities. I.A. acknowledges the Spanish Ministerio de Educación Cultura y Deporte for a FPU PhD scholarship.

■ REFERENCES

(1) Blumberger, J. *Chem. Rev.* **2015**, *115*, 11191.
(2) Nitzan, A.; Ratner, M. A. *Science* **2003**, *300*, 1384.
(3) Choi, S. H.; Kim, B.; Frisbie, C. D. *Science* **2008**, *320*, 1482.
(4) Lu, Q.; Liu, K.; Zhang, H.; Du, Z.; Wang, X.; Wang, F. *ACS Nano* **2009**, *3*, 3861.
(5) Moreno-García, P.; Gulcur, M.; Manrique, D. Z.; Pope, T.; Hong, W.; Kaliginedi, V.; Huang, C.; Batsanov, A. S.; Bryce, M. R.; Lambert, C.; Wandlowski, T. *J. Am. Chem. Soc.* **2013**, *135*, 12228.
(6) Kaliginedi, V.; Moreno-García, P.; Valkenier, H.; Hong, W.; García-Suárez, V. M.; Buiter, P.; Otten, J. L. H.; Hummelen, J. C.; Lambert, C. J.; Wandlowski, T. *J. Am. Chem. Soc.* **2012**, *134*, 5262.
(7) Luo, L.; Choi, S. H.; Frisbie, C. D. *Chem. Mater.* **2011**, *23*, 631.
(8) Choi, S. H.; Risko, C.; Ruiz-Delgado, M. C.; Kim, B.; Brédas, J. L.; Frisbie, C. D. *J. Am. Chem. Soc.* **2010**, *132*, 4358.
(9) Hines, T.; Diez-Perez, I.; Hihath, J.; Liu, H.; Wang, Z. S.; Zhao, J.; Zhou, G.; Müllen, K.; Tao, N. *J. Am. Chem. Soc.* **2010**, *132*, 11658.
(10) Sukegawa, J.; Schubert, C.; Zhu, X.; Tsuji, H.; Guldi, D. M.; Nakamura, E. *Nat. Chem.* **2014**, *6*, 899.
(11) Ricks, A. B.; Brown, K. E.; Wenninger, M.; Karlen, S. D.; Berlin, Y. A.; Co, D. T.; Wasielewski, M. R. *J. Am. Chem. Soc.* **2012**, *134*, 4581.
(12) Gilbert, M.; Albinsson, B. *Chem. Soc. Rev.* **2015**, *44*, 845.
(13) Heckmann, A.; Lambert, C. *Angew. Chem., Int. Ed.* **2012**, *51*, 326.
(14) Sedó, J.; Ruiz, D.; Vidal-Gancedo, J.; Rovira, C.; Bonvoisin, J.; Launay, J. P.; Veciana, J. *Adv. Mater.* **1996**, *8*, 748.
(15) Elsner, O.; Ruiz-Molina, D.; Vidal-Gancedo, J.; Rovira, C.; Veciana, J. *Nano Lett.* **2001**, *1*, 117.
(16) Lloveras, V.; Vidal-Gancedo, J.; Figueira-Duarte, T. M.; Nierengarten, J.-F.; Novoa, J. J.; Mota, F.; Ventosa, N.; Rovira, C.; Veciana, J. *J. Am. Chem. Soc.* **2011**, *133*, 5818.
(17) Jestin, I.; Frère, P.; Blanchard, P.; Roncali, J. *Angew. Chem., Int. Ed.* **1998**, *37*, 942.
(18) Oswald, F.; Shafiqul Islam, D.-M.; El-Khouly, M. E.; Araki, Y.; Caballero, R.; de la Cruz, P.; Ito, O.; Langa, F. *Phys. Chem. Chem. Phys.* **2014**, *16*, 2443.
(19) Rodríguez-González, S.; Ruiz-Delgado, M. C.; Caballero, R.; de la Cruz, P.; Langa, F.; López-Navarrete, J. T.; Casado, J. *J. Am. Chem. Soc.* **2012**, *134*, 5675.
(20) Rovira, C.; Ruiz-Molina, D.; Elsner, O.; Vidal-Gancedo, J.; Bonvoisin, J.; Launay, J.-P.; Veciana, J. *Chem. - Eur. J.* **2001**, *7*, 240.
(21) Heinzer, J. *Mol. Phys.* **1971**, *22*, 167. *Quantum Chemistry Program Exchange*; 1972, no. 209. We thank Prof. A. Lund for a copy of this program.
(22) Rodríguez González, S.; Nieto-Ortega, B.; González Cano, R. C.; Lloveras, V.; Novoa, J. J.; Mota, F.; Vidal-Gancedo, J.; Rovira, C.; Veciana, J.; del Corro, E.; Taravillo, M.; Baonza, V. G.; López Navarrete, J. T.; Casado, J. *J. Chem. Phys.* **2014**, *140*, 164903.
(23) Ricks, A. B.; Brown, K. E.; Wenninger, M.; Karlen, S. D.; Berlin, Y. A.; Co, D. T.; Wasielewski, M. R. *J. Am. Chem. Soc.* **2012**, *134*, 4581.
(24) Berlin, Y. A.; Ratner, M. A. *Radiat. Phys. Chem.* **2005**, *74*, 124.
(25) Petrov, E. G.; Shevchenko, Y. V.; May, V. *Chem. Phys.* **2003**, *288*, 269.
(26) Weller, A. *Z. Phys. Chem.* **1982**, *133*, 93.
(27) Apperloo, J. J.; Raimundo, J.-M.; Frère, P.; Roncali, J.; Janssen, R. A. J. *Chem. - Eur. J.* **2000**, *6*, 1698.
(28) Ratera, I.; Veciana, J. *Chem. Soc. Rev.* **2012**, *41*, 303.
(29) Kubas, A.; Gajdos, F.; Heck, A.; Oberhofer, H.; Elstner, M.; Blumberger, J. *Phys. Chem. Chem. Phys.* **2015**, *17*, 14342.
(30) Renz, M.; Theilacker, K.; Lambert, C.; Kaupp, M. *J. Am. Chem. Soc.* **2009**, *131*, 16292.
(31) Perdew, J. P.; Burke, K.; Ernzerhof, M. *Phys. Rev. Lett.* **1996**, *77*, 3865.
(32) Frisch, M. J.; Trucks, G. W.; Schlegel, H. B.; Scuseria, G. E.; Robb, M. A.; Cheeseman, J. R.; Scalmani, G.; Barone, V.; Mennucci, B.; Petersson, G. A.; Nakatsuji, H.; Caricato, M.; Li, X.; Hratchian, H. P.; Izmaylov, A. F.; Bloino, J.; Zheng, G.; Sonnenberg, J. L.; Hada, M.; Ehara, M.; Toyota, K.; Fukuda, R.; Hasegawa, J.; Ishida, M.; Nakajima, T.; Honda, Y.; Kitao, O.; Nakai, H.; Vreven, T.; Montgomery, J. A., Jr.; Peralta, J. E.; Ogliaro, F.; Bearpark, M.; Heyd, J. J.; Brothers, E.; Kudin, K. N.; Staroverov, V. N.; Kobayashi, R.; Normand, J.; Raghavachari, K.;

DOI: 10.1021/jacs.6b08649
J. Am. Chem. Soc. 2017, 139, 686−692

Rendell, A.; Burant, J. C.; Iyengar, S. S.; Tomasi, J.; Cossi, M.; Rega, N.; Millam, J. M.; Klene, M.; Knox, J. E.; Cross, J. B.; Bakken, V.; Adamo, C.; Jaramillo, J.; Gomperts, R.; Stratmann, R. E.; Yazyev, O.; Austin, A. J.; Cammi, R.; Pomelli, C.; Ochterski, J. W.; Martin, R. L.; Morokuma, K.; Zakrzewski, V. G.; Voth, G. A.; Salvador, P.; Dannenberg, J. J.; Dapprich, S.; Daniels, A. D.; Farkas, O.; Foresman, J. B.; Ortiz, J. V.; Cioslowski, J.; Fox, D. J. *Gaussian 09*, revision A.08; Gaussian, Inc.: Wallingford, CT, 2009.

(33) Bussi, G.; Donadio, D.; Parrinello, M. *J. Chem. Phys.* **2007**, *126*, 014101.

(34) Blum, V.; Gehrke, R.; Hanke, F.; Havu, P.; Havu, V.; Ren, X.; Reuter, K.; Scheffler, M. *Comput. Phys. Commun.* **2009**, *180*, 2175.

(35) Alcón, I.; Bromley, S. T. *RSC Adv.* **2015**, *5*, 98593.

DOI: 10.1021/jacs.6b08649
J. Am. Chem. Soc. 2017, 139, 686−692